Technical Reference on Hydrogen Compatibility of Materials

Austenitic Stainless Steels:
A-286 (code 2301)

Prepared by:
C. San Marchi, Sandia National Laboratories

Editors
C. San Marchi
B.P. Somerday
Sandia National Laboratories

This report may be updated and revised periodically in response to the needs of the technical community; up-to-date versions can be requested from the editors at the address given below. The success of this reference depends upon feedback from the technical community; please forward your comments, suggestions, criticisms and relevant public-domain data to:

Sandia National Laboratories
Matls Tech Ref
C. San Marchi (MS-9402)
7011 East Ave
Livermore CA 94550.

This document was prepared with financial support from the Safety, Codes and Standards program element of the Hydrogen, Fuel Cells and Infrastructure program, Office of Energy Efficiency and Renewable Energy; Pat Davis is the manager of this program element. Sandia is a multiprogram laboratory operated by Sandia Corporation, a Lockheed Martin Company, for the United States Department of Energy under contract DE-AC04-94AL85000.

1. General

A-286 is an iron-base superalloy commonly used for its combination of high-strength and good corrosion resistance at intermediate temperatures. The high-nickel content of A-286 and its sister alloys make them resistant to strain-induced phase transformations. Although also referred to as stainless steel, A-286 is considerably different from the 300-series alloys in that it is strengthened by precipitation of the γ' phase, $Ni_3(Al,Ti)$ [1]. Although A-286 can be welded (material specifications exist for welding grades of A-286, e.g. [2]), a modified version of the alloy, called JBK-75, was developed to improve its weldability as well as improve hydrogen compatibility [3]. NASA has developed an alloy called NASA-HR-1, which is based on JBK-75, to improve strength as well as resistance to hydrogen embrittlement, oxidation and corrosion [4]. NASA-HR-1 should not be confused with the Chinese alloy HR-1, which is similar to type 316 stainless steel [5].

The high-nickel and chromium content of the A-286 family of alloys implies high stacking fault energy [6], a characteristic associated with uniform plastic deformation and consequently resistance to hydrogen embrittlement in austenitic stainless steels [7, 8]. The coherent interface of the γ' precipitates in A-286 and JBK-75, on the hand, tends to enable non-uniform plastic deformation, a feature in austenitic steels that is often used to explain comparatively poor resistance to hydrogen embrittlement [6, 9]. The uniformity of plastic deformation in precipitation strengthened austenitic alloys, however, may be less important in governing hydrogen embrittlement compared to other metallurgical features, such as internal interfaces and second phases that can interact with internal hydrogen.

Two general observations distinguish hydrogen-assisted fracture in the A-286 family of alloys from the single-phase austenitic stainless alloys: (i) A-286 that has been tested in tension in external hydrogen gas is not embrittled [6, 10-14], while A-286 with internal hydrogen (by thermal precharging in hydrogen gas) features a significant reduction in tensile ductility [3, 6, 9, 15], and (ii) JBK-75 (internal hydrogen) and A-286 (external hydrogen) that have been tested at elevated strain rates in tension do not show an increase in ductility compared to low strain rates [14, 16]. These observations could be explained by the tenacious oxide that forms upon aging A-286 (even when aged in reducing environment), which acts as a permeation barrier during the relatively short exposure of tensile tests, if these tensile specimens were machined prior to aging. The presence of an oxide, however, cannot explain the strain rate experiments of Holbrook and West on thermally precharged JBK-75, which showed no strain rate effect. Holbrook and West suggested that interactions between hydrogen and dislocations may be different in JBK-75 compared to single-phase austenitic alloys [16].

The mechanisms that contribute to hydrogen embrittlement in the A-286 family of superalloys have not been firmly established. It has been speculated that loss of matrix-γ precipitate coherency during deformation allows hydrogen to accumulate at these incoherent interfaces leading to hydrogen-assisted fracture [6]. Observations of smaller dimple size in the presence of internal hydrogen [6] support the view that hydrogen assists nucleation of microvoids, perhaps at newly incoherent interfaces. Ductile microvoid coalescence, however, competes with intergranular fracture in these alloys in the presence of hydrogen. Intergranular fracture is more prevalent and features less evidence of ductile fracture processes in materials aged for longer times as the number and size of grain-boundary precipitates increases with time [3, 17].

Intergranular fracture is generally attributed to the presence of η-phase (Ni_3Ti), which precipitates primarily on or near grain boundaries during aging. Heat treatments (and compositional gradients as in welds), for example, that promote precipitation of the η-phase result in higher crack growth rates and lower threshold stress intensity factors in sustained-loading fracture specimens that have been tested in high-pressure gaseous hydrogen [18, 19]. Ductility losses, as determined from tensile tests, however, do not show a dependence on the volume fraction of the η-phase, nor on the degree of intergranular fracture [3, 17]. It has been surmised that failure of tensile specimens in the presence of hydrogen is dominated by crack nucleation in these alloys, and once a crack forms it propagates rapidly along susceptible features such as grain boundaries [17]. For example, precracked tensile specimens of JBK-75 tested in hydrogen gas failed entirely by intergranular fracture, while smooth tensile specimens of the same material in the same conditions failed by microvoid coalescence [13].

While the nature of interactions between hydrogen, dislocations, and the various precipitates in the A-286 family of alloys are not unequivocally known, the data suggest that shorter aging times and lower aging temperatures result in microstructures that are less susceptible to hydrogen effects [3, 17-20]. Fusion weld microstructures may be particularly susceptible to hydrogen because titanium and nickel segregation in the weld may facilitate precipitation of the η-phase [18, 21].

1.1 Composition

Table 1.1.1 lists the compositions of several heats of A-286 used to study hydrogen effects. Welding grades of A-286 specify low silicon and manganese, e.g. [2]. A modified version of A-286, called JBK-75, was developed to improve weldability and hydrogen compatibility [3]; the compositions of several heats of JBK-75 are listed in Table 1.1.2. More recently, JBK-75 has been modified by researchers at NASA to improve strength as well as resistance to hydrogen embrittlement, oxidation and corrosion; this alloy, NASA-HR-1, has additions of tungsten and cobalt in addition to increased nickel and molybdenum content [4].

1.2 Other designations

AISI Type 660, UNS S66286
related alloys: JBK-75 (UNS S66285), V-57, NASA-HR-1

2. Permeability and Solubility

The permeation and solubility of hydrogen in JBK-75 was found to be independent of heat treatment for conventional solution heat treating and aging cycles [22]. Permeability and solubility generally follow an Arrhenius-type relationship with temperature; Table 2.1 provides these relationships for JBK-75 as well as relationships averaged for several austenitic alloys. Plotting these relationships shows that the superalloys have nominally the same permeability and solubility as the single-phase austenitic stainless alloys, Figure 2.1 and Figure 2.2.

Hydrogen concentration measurements by hot extraction techniques show somewhat different trends from permeation studies. The hydrogen concentration was found to strongly depend on processing conditions for modified A-286 (presumably JBK-75) with internal hydrogen (thermally precharged in hydrogen gas), Table 2.2 [23]. Microstructural details that might account for the measured difference were not reported or discussed in that study. In another study [15], hydrogen concentration measurements in JBK-75 by hot extraction were reported to be 20% higher than concentrations calculated based on data for austenitic alloys. The source of these discrepancies is not clear, but may be related to additional hydrogen trapped at specific microstructural features, such as precipitate interfaces. Trapping of hydrogen is generally considered to be low in single-phase austenitic alloys, however, further study is necessary to determine if hydrogen trapping is significant in precipitation-hardened stainless steels such as the A-286 family of alloys. While hot extraction techniques determine the total hydrogen in the material, i.e., both trapped hydrogen and mobile hydrogen, the solubility and permeability only depend on lattice or mobile hydrogen, which should not be strongly affected by precipitation in A-286 based alloys [22]. Therefore, the relationships provided in Ref. [24] (when corrected to hydrogen), Table 2.1, should be considered the best conservative (high value) estimate for permeability and solubility when extrapolated to room temperature. Based on available data, an upper bound to the equilibrium concentration of hydrogen in the A-286 family of alloys can be approximated from the recommended solubility relationship.

3. Mechanical Properties: Effects of Gaseous Hydrogen

3.1 Tensile properties

3.1.1 Smooth tensile properties

Room temperature tensile testing of A-286 and JBK-75 show little or no loss in ductility during straining in hydrogen gas at pressures up to 172 MPa. Tensile specimens with internal hydrogen (by thermal precharging in hydrogen gas), however, show a significant loss in ductility, typically 50 to 60% loss in reduction in area, Tables 3.1.1.1 and 3.1.1.2. As for most austenitic stainless steels, strength of A-286 and JBK-75 is relatively unaffected by both internal and external hydrogen.

Tensile ductility of JBK-75 with internal hydrogen is reduced at room temperature but is relatively little affected at lower temperature, tensile properties are provided in Table 3.1.1.3 and Figure 3.1.1.1 from room temperature to 77 K. Near room temperature JBK-75 with internal hydrogen exhibits very little ductility after necking begins, but ductility is greater at both lower temperature and elevated temperature. This is shown in Figure 3.1.1.2 for two sets of data, the lower curve represents the relative reduction in area after necking (RRA*) [16], while the upper curve is the RRA as typically reported from total plastic strain for data from Table 3.1.1.3. In all cases the ductility and evidence of ductile fracture processes increase at lower temperature [16, 20].

Unlike other stainless steels in the presence of hydrogen, ductility in JBK-75 is not recovered at elevated strain rate up to 0.06 s^{-1}, Figure 3.1.1.3; the data from Ref. [16] is given as the relative reduction in area after necking (RRA*).

Aging tensile specimens after machining results in enhanced precipitation of the γ' phase due to surface deformation and a microstructure that is more sensitive to hydrogen, Table 3.1.1.4 [15], see also section 4.2.

3.1.2. Notched tensile properties

Notched tensile specimens show essentially no difference in properties when tested in helium or hydrogen at pressures up to 69 MPa, Table 3.1.2.1. The strength of notched tensile specimens of JBK-75 is unaffected by internal hydrogen for temperatures from 77 K to room temperature; the reduction in area of notched tensile specimens, however, is reduced somewhat at room temperature but relatively unaffected at low temperature, Figure 3.1.2.1.

In a separate study, A-286 was electrolytically precharged with internal hydrogen from a molten salt bath to various uniform hydrogen concentrations up to 40 wppm [25]. The notched tensile properties were then measured on single-edge-notched specimens. At a hydrogen concentration of 40 wppm, the notched tensile strength decreased by about 20% and the reduction in area decreased by 50%. The reported ductility loss near 25 wppm [25] is similar to that reported at room temperature for JBK-75 with internal hydrogen incorporated by thermal precharging from hydrogen gas as reported in Ref [20] (and shown in Figure 3.1.2.1).

3.2 Fracture mechanics

3.2.1 Fracture toughness

The fracture toughness of JBK-75 decreased by about half for material with high concentrations of internal hydrogen (>100 wppm), Table 3.2.1.1. Both ductile features and intergranular separation were observed on JBK-75 fracture surfaces [26]; however, uncharged materials primarily featured fracture modes consistent with ductile processes, while intergranular failure was more prevalent in specimens with internal hydrogen. Void nucleation was observed at grain boundaries, but evidence of ductile void formation was less in materials with greater volumes of grain boundary η-phase [26]. The η-phase was present on grain boundaries for all conditions tested, but the longer heat treatments resulted in greater volumes of η-phase, especially at the grain boundaries, and lower fracture toughness for materials with and without internal hydrogen [26].

Fracture toughness was determined [27] from 25.4 mm (1 in) thick, wedge open loading (WOL) specimens in constant displacement tests that did not meet plane strain requirements of standardized testing procedures [28]. These data are provided only as qualitative indicators since there is no other data reported in the literature for fracture toughness of A-286 or JBK-75 in external hydrogen gas. In 34.5 MPa gaseous helium, fracture toughness values (K_Q) of 145 and 138 MPa m$^{1/2}$ are reported at 295 K and 144 K respectively, while in 34.5 MPa gaseous hydrogen values of 100 and 152 MPa m$^{1/2}$ are reported. The material for these tests was forged plate, heat W73 (Table 1.1.1), solution heat treated at 1255 K for 1 hour, oil-quenched and aged at 991 K for 16 hours followed by air-cooling.

3.2.2 Threshold stress intensity factor

Data from a number of austenitic stainless steels and iron-based (precipitation-strengthened) superalloys show that higher resistance to cracking under static loads in hydrogen generally corresponds to lower yield strength and similar values can be expected for a wide range of austenitic alloys [19]. Austenitic alloys with yield strengths less than about 700 MPa, in particular, have high resistance to cracking in high-pressure hydrogen gas environments under static loads [19]. Threshold stress intensity factor (K_{TH}) data for JBK-75 in high-pressure hydrogen gas, however, indicate that some microstructures are more susceptible than others, Table 3.2.2.1. Microstructure is especially important in two-phase alloy systems such as A-286, JBK-75 and other precipitation-strengthened alloys. In all cases, intergranular separation as well as ductile fracture processes were apparent from the fracture surfaces, with the fraction of ductile features scaling with threshold stress intensity factor. In addition, greater precipitation of η-phase in the grain boundary correlated with lower threshold [18]. The relatively low threshold stress intensity factor of the solution heat treated JBK-75 aged at the highest temperature is attributed to precipitation of η-phase at grain boundaries [18]. Compositional segregation in fusion-welded material also contributes to increased hydrogen susceptibility in these K_{TH} measurements [18, 19, 21].

In an earlier study, measurements of K_{TH} were attempted on 25.4 mm thick wedge open loading (WOL) specimens of A-286 that were not precracked and were loaded beyond the yield point [27]. None of the testing conditions satisfied the plane strain requirement of standardized testing procedures [28]. These data are provided for qualitative comparison. In 34.5 MPa gaseous hydrogen at room temperature, threshold stress intensity factor was found to be <113 MPa·m$^{1/2}$. At 144 K, no crack propagation was observed at an applied stress intensity factor of 198 MPa·m$^{1/2}$ in 34.5 MPa gaseous hydrogen. The material for these tests was forged plate, heat W73 (Table 1.1.1), solution heat treated at 1255 K for 1 hour, oil-quenched and aged at 991 K for 16 hours followed by air cooling.

The effect of external hydrogen on crack growth in sustained loading of surface-flawed thin dog-bone-like specimens of A-286 is reported to be negligible in 6.9 MPa gaseous hydrogen [29].

The threshold stress intensity factor for crack propagation of fatigue precracked A-286, with internal hydrogen from electrolytic precharging in molten salt, was measured as a function of hydrogen concentrations up to 30 wppm [30]. For these specimens, however, plane-stress conditions dominated thus the data cannot be compared to standardized plane-strain values of the stress intensity factor. Nevertheless, the relative K_{TH} (internal hydrogen relative to uncharged) was found to be about 0.75 for 30 wppm hydrogen [30]. In addition, the A-286 was less affected by hydrogen than most of the tested alloys including type 301 and 304 stainless steels and nickel-base superalloys (IN625 and IN718) [30].

3.3 Fatigue

Low-cycle fatigue experiments on A-286 show essentially no effect of hydrogen gas [31]. Hollow specimens pressurized to 34 MPa hydrogen and helium gas were tested in 1% total strain range and failed at approximately 2800 cycles.

3.4 Creep

Stress rupture tests in hydrogen gas at 922 K and a stress of 390 MPa result in a reduction in lifetime of about 20% for A-286, from 264 hours in 3.4 MPa air to 215 hours in 3.4 MPa hydrogen gas [31]. A large variation is associated with the rupture times in hydrogen.

3.5 Impact
Charpy impact tests on EB-welded JBK-75 joints show some sensitivity to internal hydrogen (by thermal precharging from hydrogen gas) [32], see section 4.3.

3.6 Disk rupture tests
Disk rupture tests at room temperature show that A-286 is unaffected by pressurized hydrogen [33, 34]. Low-cycle fatigue in the disk rupture configuration (40 cycles to 0.5 of the rupture pressure) also did not affect the rupture pressure in hydrogen [34]. In a later report, disk rupture tests on JBK-75 and A-286 equivalent alloys showed considerable hydrogen embrittlement except in the solution heat-treated condition [35]. Rupture pressures for hydrogen were almost half of the rupture pressures in helium and evidence of intergranular failure modes were explained by η-phase precipitation at grain boundaries.

At elevated temperatures (360 to 700 K), hydrogen gas reduces the rupture pressure compared to helium gas. Exposure to hydrogen gas at 8.6 MPa for 48 hours further reduces the rupture pressure when pressurized by hydrogen gas [33]. This data underscores the importance of delayed effects due to hydrogen uptake and diffusion in metals.

4. Metallurgical Considerations

4.1 Primary processing
Carbide and sulfide inclusions are believed to have a significant impact on the fracture toughness of JBK-75 in the presence of hydrogen [36]. Deformation and thermomechanical processing accelerate the aging response of A-286 and JBK-75 [15, 17].

4.2 Heat treatment

Since A-286 and alloys based on A-286 are precipitation-strengthened, the heat treatment is of primary importance for controlling microstructure and therefore, controlling strength and susceptibility to hydrogen embrittlement. Lower aging temperatures may help control precipitation kinetics and reduce the formation of undesirable phases such the η-phase [17]. The typical aging cycle for A-286 is 16 hours at 993 K. A two-step aging process is often employed for JBK-75: 8 hours at 948 K, followed by 8 hours at 873 K.

A-286 and JBK-75 in the solution heat-treated condition show little ductility loss in tensile tests with internal hydrogen, Figure 4.2.1. Aging results in a significant reduction in ductility due to η-phase precipitation and this reduction is exacerbated in the presence of internal hydrogen [3, 17]. This ductility loss is essentially independent of aging times greater than a few hours, although the volume fraction of η-phase increases substantially as does the fraction of intergranular failure [3].

Deformation induced by machining has been shown to accelerate η-phase precipitation in A-286, leading to a microstructure that is more susceptible to hydrogen embrittlement, Table 3.1.1.4 [15]. Similarly, intentional cold work accelerates the aging response of JBK-75 and results in ductility loss for aging times as short as one hour with internal hydrogen, Figure 4.2.1. These data indicate that substantially shorter aging times may offer improved hydrogen compatibility without significant compromise on strength, and that standard aging cycles (993K for 16 hours) are not appropriate for thermomechanically processed materials for service in hydrogen. Values of fracture toughness [26], Table 3.2.1.1, and threshold stress intensity factor in gaseous hydrogen [19], Table 3.2.2.1, also support the principle that shorter aging times and lower temperatures result in improved hydrogen compatibility.

4.3 Properties of welds

Tensile testing of JBK-75 gas tungsten arc (GTA) welds with high concentrations of internal hydrogen show significant losses in ductility [21]. Interdentritic regions in these welds are rich in titanium and nickel, and thus believed to be preferential sites for precipitation of the η-phase (Ni_3Ti) and vulnerable to intergranular fracture [6, 17, 18]. Fracture of the welds was primarily by microvoid coalescence with some evidence of the underlying weld microstructure, however, localized regions of intergranular fracture were observed near the surface of specimens with internal hydrogen, i.e. in regions where the hydrogen concentration was greatest. As in base material [6], the dimple size was reduced in the presence of hydrogen, presumably due to increased activation of nucleation sites, for example in the interdentritic regions. The tensile properties of GTA welds are listed in Table 4.3.1. These data are shown for reference only as they represent the properties of a composite specimen (fusion zone, heat-affected zone and base metal), however, they do demonstrate the effect of hydrogen on the ductility of the welds.

The threshold stress intensity factor of a fusion weld of JBK-75 in hydrogen was reported to be about half that measured for similarly aged forged base metal [19], Table 3.2.2.1. The increased susceptibility is attributed to the macrosegregation inherent to fusion welding processes.

Like the single-phase austenitic stainless steels, the susceptibility to hydrogen embrittlement (as measured by tensile ductility) of JBK-75 electron-beam (EB) welded joints reaches a minimum near room temperature for material with internal hydrogen [32], Table 4.3.2 and Figure 4.3.1. Charpy impact tests, however, show the greatest susceptibility to hydrogen embrittlement at lower temperature and only a nominal effect at room temperature [32]. Overaging these welded joints (30 h at 1013 K) increases susceptibility to hydrogen embrittlement, due to η-phase precipitation [32].

5. References

1. WD Klopp. Nickel Chromium Steels: Fe-25Ni-15Cr-2Ti-1.5Mn-1.3Mo-0.3V (code 1601). in: WF Brown, H Mindlin and CY Ho, editors. Aerospace Structural Metals Handbook. West Lafayette: CINDAS/USAF CRDA Handbooks Operation, Purdue University (1987).
2. AMS 5895C, Steel, Corrosion, and Heat Resistant, Bars, Wire, Forgings, Tubing, and Rings, 15Cr - 25.5Ni - 1.2Mo - 2.1Ti - 0.006B - 0.30V, Consumable Electrode Melted, 1750˚F (954˚C) Solution Heat Treated, Welding Grade, Precipitation Hardenable (UNS S66286). Society of Automotive Engineers (2000).
3. JA Brooks and AW Thompson. Microstructure and Hydrogen Effects on Fracture in the Alloy A-286. Metall Trans 24A (1993) 1983-1991.

4. PS Chen, B Panda and BN Bhat. NASA-HR-1, a New Hydrogen-Resistant Fe-Ni Base Superalloy. in: AW Thompson and NR Moody, editors. Proceedings of the Fifth International Conference on the Effect of Hydrogen on the Behavior of Materials: Hydrogen Effects in Materials, 1994, Moran WY. TMS, Warrendale PA (1996) p. 1011-1019.
5. J Qian, J Chen, J Chen, Z Xu, W Wang and C Pan. Corrosion of austenitic stainless steel in liquid lithium. J Nucl Mater 179-181 (1991) 603-606.
6. AW Thompson and JA Brooks. Hydrogen Performance of Precipitation-Strengthened Stainless Steels Based on A-286. Metall Trans 6A (1975) 1431-1442.
7. MR Louthan, GR Caskey, JA Donovan and DE Rawl. Hydrogen Embrittlement of Metals. Mater Sci Eng 10 (1972) 357-368.
8. BC Odegard, JA Brooks and AJ West. The Effect of Hydrogen on Mechanical Behavior of Nitrogen-Strengthened Stainless Steel. in: AW Thompson and IM Bernstein, editors. Proceedings of an International Conference on Effect of Hydrogen on Behavior of Materials, 1975, Moran WY. The Metallurgical Society of AIME (1976) p. 116-125.
9. AW Thompson. Ductility Losses in Austenitic Stainless Steels Caused by Hydrogen. in: IM Bernstein and AW Thompson, editors. Proceedings of the International Conference on the Effects of Hydrogen on Materials Properties and Selection and Structural Design: Hydrogen in Metals, 1973, Champion PA. American Society of Metals (1974) p. 91-105.
10. RJ Walter and WT Chandler. Effects of High-Pressure Hydrogen on Metals at Ambient Temperature: Final Report (NASA CR-102425). Rocketdyne (report no. R-7780-1) for the National Aeronautics and Space Administration, Canoga Park CA (February 1969).
11. AW Thompson. Hydrogen-Induced Ductility Loss in Commercial Precipitation-Strengthened Stainless Steels. Metall Trans 7A (1976) 315-318.
12. TL Capeletti and MR Louthan. The Tensile Ductility of Austenitic Steels in Air and Hydrogen. J Eng Mater Technol 99 (1977) 153-158.
13. RE Stoltz and AJ West. Hydrogen Assisted Fracture in FCC Metals and Alloys. in: IM Bernstein and AW Thompson, editors. Proceedings of the International Conference on Effect of Hydrogen on Behavior of Materials: Hydrogen Effects in Metals, 1980, Moran WY. The Metallurgical Society of AIME (1980) p. 541-553.
14. EJ Vesely, RK Jacobs, MC Watwood and WB McPherson. Influence of Strain Rate on Tensile Properties in High-Pressure Hydrogen. in: AW Thompson and NR Moody, editors. Proceedings of the Fifth International Conference on the Effect of Hydrogen on the Behavior of Materials: Hydrogen Effects in Materials, 1994, Moran WY. TMS, Warrendale PA (1996) p. 363-374.
15. JA Brooks and MR Louthan. Surface Preparation and Hydrogen Compatibility of an Iron Base Superalloy. Metall Trans 11A (1980) 1981-1986.
16. JH Holbrook and AJ West. The Effect of Temperature and Strain Rate on the Tensile Properties of Hydrogen Charged 304L, 21-6-9, and JBK 75. in: IM Bernstein and AW Thompson, editors. Proceedings of the International Conference on Effect of Hydrogen on Behavior of Materials: Hydrogen Effects in Metals, 1980, Moran WY. The Metallurgical Society of AIME (1980) p. 655-663.
17. BC Odegard and AJ West. The Effect of eta-phase on the Hydrogen Compatibility of a Modified A-286 Superalloy: Microstructural and Mechanical Properties Observations. in: IM Bernstein and AW Thompson, editors. Proceedings of the International Conference on Effect of Hydrogen on Behavior of Materials: Hydrogen Effects in Metals, 1980, Moran WY. The Metallurgical Society of AIME (1980) p. 597-606.

18. MW Perra and RE Stoltz. Sustained-Load Cracking of a Precipitation-Strengthened Austenitic Steel in High-Pressure Hydrogen. in: IM Bernstein and AW Thompson, editors. Proceedings of the International Conference on Effect of Hydrogen on Behavior of Materials: Hydrogen Effects in Metals, 1980, Moran WY. The Metallurgical Society of AIME (1980) p. 645-653.
19. MW Perra. Sustained-Load Cracking of Austenitic Steels in Gaseous Hydrogen. in: MR Louthan, RP McNitt and RD Sisson, editors. Environmental Degradation of Engineering Materials in Hydrogen. Blacksburg VA: Laboratory for the Study of Environmental Degradation of Engineering Materials, Virginia Polytechnic Institute (1981) p. 321-333.
20. LM Ma, GJ Liang and YY Li. Effect of Hydrogen Charging on Ambient and Cryogenic Mechanical Properties of a Precipitate-Strengthened Austenitic Steel. in: FR Fickett and RP Reed, editors. Proceedings of the International Cryogenic Materials Conference, 1991, Huntsville AL. Advances in Cryogenic Engineering, vol. 38A. Plenum Press, NY (1992) p. 77-84.
21. JA Brooks, AJ West and AW Thompson. Effect of Weld Composition and Microstructure on Hydrogen Assisted Fracture of Austenitic Stainless Steels. Metall Trans 14A (1983) 75-84.
22. J Xu, XK Sun, WX Chen and YY Li. Hydrogen Permeation and Diffusion in Iron-base Superalloys. Acta metall mater 41 (1993) 1455-1459.
23. GR Caskey and RD Sisson. Hydrogen Solubility in Austenitic Stainless Steels. Scr Metall 15 (1981) 1187-1190.
24. MR Louthan and RG Derrick. Hydrogen Transport in Austenitic Stainless Steel. Corros Sci 15 (1975) 565-577.
25. PD Hicks and CJ Altstetter. Internal Hydrogen Effects on Tensile Properties of Iron- and Nickel-Base Superalloys. Metall Trans 21A (1990) 365-372.
26. BC Odegard, SL Robinson and NR Moody. Effects of Internal Hydrogen on the Toughness and Fracture of Forged JBK-75 Stainless Steel. in: AW Thompson and NR Moody, editors. Proceedings of the Fifth International Conference on the Effect of Hydrogen on the Behavior of Materials: Hydrogen Effects in Materials, 1994, Moran WY. TMS, Warrendale PA (1996) p. 591-598.
27. RJ Walter and WT Chandler. Influence of Gaseous Hydrogen on Metals: Final Report (NASA CR-124410). Rocketdyne for the National Aeronautics and Space Administration, Canoga Park CA (Oct 1973).
28. ASTM E 1681-99, Standard Test Method for Determining Threshold Stress Intensity Factor for Environment-Assisted Cracking of Metallic Materials. American Society for Testing and Materials (1999).
29. RG Forman. Environmental Crack-Growth Behavior of High-Strength Pressure Vessel Alloys (NASA TN D-7952). Lyndon B. Johnson Space Center, National Aeronautics and Space Administration, Houston TX (Apr 1975).
30. PD Hicks and CJ Altstetter. Hydrogen-Enhanced Cracking of Superalloys. Metall Trans 23A (1992) 237-249.
31. RP Jewitt, RJ Walter, WT Chandler and RP Frohmberg. Hydrogen Environment Embrittlement of Metals (NASA CR-2163). Rocketdyne for the National Aeronautics and Space Administration, Canoga Park CA (March 1973).
32. YY Li, LM Ma, GJ Liang, QH Gui and ZK Li. Effect of Hydrogen on Mechanical Properties of EB-Welded Joints of JBK-75 Steel from Ambient to Cryogenic Temperatures. in: RP Reed, FR Fickett, LT Summers and M Stieg, editors. Proceedings of the International

Cryogenic Materials Conference, 1993, Albuquerque NM. Advances in Cryogenic Engineering, vol. 40B. Plenum Press, NY (1994) p. 1283-1289.
33. J Papp, RF Hehemann and AR Troiano. Hydrogen Embrittlement of High Strength FCC Alloys. in: IM Bernstein and AW Thompson, editors. Proceedings of the International Conference on the Effects of Hydrogen on Materials Properties and Selection and Structural Design: Hydrogen in Metals, 1973, Champion PA. American Society for Metals (1974) p. 657-669.
34. J-P Fidelle, R Bernardi, R Broudeur, C Roux and M Rapin. Disk Pressure Testing of Hydrogen Environment Embrittlement. in: Hydrogen Embrittlement Testing, ASTM STP 543, American Society for Testing and Materials. (1974) p. 221-253.
35. PF Azou and JP Fidelle. Very low strain rate hydrogen gas embrittlement (HGE) and fractography of high-strength, mainly austenitic stainless steels. in: MR Louthan, RP McNitt and RD Sisson, editors. Environmental Degradation of Engineering Materials III, 1987, The Pennsylvania State University, University Park PA. The Pennsylvania State University, University Park PA p. 189-198.
36. NR Moody, SL Robinson and WM Garrison. Austenitic Superalloy Selection and Development for Hydrogen Service from a Microstructure Perspective. in: HJ Cialoni, ME Blum, GWE Johnson and GF VanderVoort, editors. Proceedings of the Twentieth Annual Technical Meeting of the International Metallographic Society: Metallography of Advanced Materials, 1987, Monterey CA. Microstructural Science, vol. 16. ASM, Metals Park OH (1988) p. 177-192.
37. ASTM DS-56H, Metals and Alloys in the UNIFIED NUMBERING SYSTEM (SAE HS-1086 OCT01). American Society for Testing and Materials (Society of Automotive Engineers) (2001).
38. XK Sun, J Xu and YY Li. Hydrogen Permeation Behaviour in Austenitic Stainless Steels. Mater Sci Eng A114 (1989) 179-187.
39. T-P Perng and CJ Altstetter. Effects of Deformation on Hydrogen Permeation in Austenitic Stainless Steels. Acta metall 34 (1986) 1771-1781.
40. SL Robinson and NR Moody. The Effect of Hydrogen, Tritium and Decay Helium on the Fracture Toughness of a Stainless Steel Superalloy. J Nucl Mater 140 (1986) 245-251.
41. RE Stoltz, NR Moody and MW Perra. Microfracture Model for Hydrogen Embrittlement of Austenitic Steels. Metall Trans 14A (1983) 1528-1531.

Table 1.1.1. Specification limits for A-286 and composition of several heats of A-286 stainless steel used to study hydrogen effects.

heat	Fe	Cr	Ni	Ti	Mn	Mo	V	Al	Si	C	B	other	Ref.
UNS S66286	Bal	13.50 16.00	24.0 27.0	1.90 2.35	2.00 max	1.00 1.50	0.10 0.50	0.35 max	1.00 max	0.08 max	0.0010 0.010	0.40 max P; 0.030 max S	[37]
W69	Bal	15.07	25.58	1.93	1.47	1.35	0.30	0.13	0.61	0.052	0.0055	0.019 P; 0.010 S	[10]
W73	Bal	14.15	24.88	2.21	1.20	1.25	0.22	0.16	0.63	0.048	0.47	0.010 S; 0.016 P; 0.01 Zr	[27]
P81	Bal	14.0	24.33	2.15	0.13	1.16	---	---	0.16	0.054	---		[19]
B93	Bal	14.90	24.93	2.15	1.32	1.25	0.21	0.19	0.63	0.068	0.004	0.003 S; 0.018 P	[3]
V96	Bal	14.02	24.38	2.09	0.28	1.37	0.2	0.13	0.22	0.024	0.0046	0.1 Cu; 0.08 Co; 0.001 S; 0.001 P	[14]
V-57	Bal	14.8	26.0	3.0	0.3	1.25	0.3	0.25	0.6	0.05	0.01	Nominal values for alloy V-57	[11]

Table 1.1.2. Specification limits for JBK-75 and composition of several heats of JBK-75 stainless steel used to study hydrogen effects.

heat	Fe	Cr	Ni	Ti	Mn	Mo	V	Al	Si	C	B	other	Ref.
UNS S66286	Bal	13.50 16.00	29.00 31.00	2.0 2.3	0.20 max	1.00 1.50	0.10 0.50	0.15 0.35	0.10 max	0.01 0.03	0.002 max	0.006 max S; 0.010 max P	
T75	Bal	14.48	30.46	2.07	0.11	1.22	0.25	0.27	0.15	0.020	0.0010		[6]
B80	Bal	14.02	29.58	2.10	<0.01	1.28	0.35	0.16	<0.01	0.019	<0.001		[15]
O80	Bal	15.3	29.8	2.1	0.011	1.2	0.42	0.3	0.075	0.012	0.0011	0.004 S; 0.01 P	[17]
P80	Bal	15.5	30.7	2.1	0.053	1.2	0.26	0.2	0.032	0.017	<0.0005	0.0013 S; <0.002 P	[19]
B83w	Bal	15.0	30.0	2.2	0.1	1.2	---	0.2	0.1	0.03	0.001	0.01 S; 0.01 P	[21]
X93	Bal	15.22	29.48	1.85	0.19	1.53	0.26	0.20	0.17	0.024	0.0019	0.004 S; 0.011 P	[22]

w = composition of the weld fusion zone

Table 2.1. Permeability and solubility relationships for JBK-75 and average relationships determined for several austenitic stainless steels.

Material	Temperature Range (K)	Pressure Range (MPa)	$\Phi = \Phi_o \exp(-E_\Phi / RT)$		$S = S_o \exp(-E_S / RT)$		Ref.
			Φ_o $\left(\frac{\text{mol H}_2}{\text{m} \cdot \text{s} \cdot \sqrt{\text{MPa}}}\right)$	E_Φ $\left(\frac{\text{kJ}}{\text{mol}}\right)$	S_o $\left(\frac{\text{mol H}_2}{\text{m}^3 \cdot \sqrt{\text{MPa}}}\right)$	E_S $\left(\frac{\text{kJ}}{\text{mol}}\right)$	
JBK-75, heat X93	483-703	0.1	4.36×10^{-4}	62.10	145	13.58	[22]
Average of several austenitic alloys †	423-700	0.1-0.3	1.2×10^{-4}	59.8	179	5.9	[24]
Average of six austenitic alloys	473-703	0.1	2.81×10^{-4}	62.27	488	8.65	[38]
Average of four austenitic alloys	373-623	$1\text{x}10^{-4}$-0.03	5.35×10^{-5}	56.1	266	6.86	[39]

† Data from Ref. [24] is determined for deuterium: permeability has been corrected here to give permeability of hydrogen (by multiplying by the square root of the mass ratio: √2); solubility is assumed to be independent of isotope.

Table 2.2. Hydrogen concentration of modified A-286 alloys measured using hot extraction after thermal precharging in hydrogen gas.

Material	Surface condition	Thermal precharging	Hydrogen concentration		Ref.
			wppm	appm	
JBK-75 ST + A	---	69 MPa H_2 573 K	54	3000	[16]
"modified A-286" Annealed	600 grit finish	69 MPa H_2 470 K	80	4500	[23]
	Electropolished		81	4500	
"modified A-286" HERF	600 grit finish		51	2900	
	Electropolished		55	3100	
JBK-75 ST + A	---	10 MPa H_2 573 K	25	1400	[20]

HERF = high energy rate forging, ST = solution treatment, A = age

Table 3.1.1.1. Smooth tensile properties of A-286 stainless steel at room temperature; measured in external hydrogen gas or with internal hydrogen (measured in air after thermal precharging in hydrogen gas).

Material	Thermal precharging	Test environment	Strain rate (s^{-1})	S_y (MPa)	S_u (MPa)	El_u (%)	El_t (%)	RA (%)	Ref.
A-286	None	69 MPa He	---	724	1117	---	26	47	[12]
	None	69 MPa H_2		710	1131	---	34	49	
A-286, heat W69 ST + A (1173K/2h + 993K/16h)	None	69 MPa He	0.67 x 10^{-3}	848	1089	---	26	44	[10, 31]
	None	69 MPa H_2		---	1117	---	29	43	
A-286 A (990K/16h)	None	Air	---	760†	1065	---	21	32	[6, 9]
	None	69 MPa H_2		---	---	(RRA ~ 1)			
	(1)	Air		---	---	(RRA ~ 0.5)			
A-286 HERF + A (990K/16h)	None	Air	---	850†	1105	---	---	(30)	[9]
	None	69 MPa H_2		---	---	(RRA ~ 1)			
	(1)	Air		---	---	(RRA ~ 0.5)			
A-286 HERF	None	Air	---	440†	750	---	---	(58)	[9]
	(1)	Air		---	---	(RRA ~ 1)			
A-286, heat V96 ST + A (1266K/1h/WQ+ 994K/16h/AC)	None	34 MPa He	8.3 x 10^{-6}	843	1166	24	---	50	[14]
	None	34 MPa H_2		839	1159	24	---	51	
V-57, heat V-57 ST + A (1255K/2h/OQ+ 990K/16h/AC)	None	Air	---	690	1145		32	50	[11]
	None	69 MPa H_2		---	---	(RRA ~ 0.95)			
	(3)	Air		---	---	(RRA ~ 0.25)			

Values in parenthesis are determined from plots.
HERF = high energy rate forging, ST = solution treatment, A = age, WQ = water quench, OQ = oil quench, AC = air cool
† stress at 0.2% strain
(1) 69 MPa hydrogen, 475 K, 1500 h
(2) 24 MPa hydrogen, 475 K, 400 h (gauge diameter = 6.5 mm diameter)

Table 3.1.1.2. Smooth tensile properties of JBK-75 stainless steel at room temperature; measured in external hydrogen gas, or with internal hydrogen (measured in air after thermal precharging in hydrogen gas).

Material	Thermal precharging	Test environment	Strain rate† (s^{-1})	S_y (MPa)	S_u (MPa)	El_u (%)	El_t (%)	RA (%)	Ref.
JBK-75, heat T75 ST + A (1200K/2h + 990K/16h/AC)	None	Air		875	1305		21	55	[6]
	None	69 MPa H_2	---	---	---	RRA ~ 1			
	(1)	air		---	---	RRA ~ 0.9			
JBK-75, heat P80 A (993K/16h)	None	Air	0.021 mm/s†	717	1131	---	28	51	[13]
	None	172 MPa H_2		---	---	---	---	47	
JBK-75, heat B80 A (993K/16h)	None	Air	0.33 x 10^{-3}	702	1105	18	23	45	[15]
	(2)	Air		703	1100	16	17	20	
JBK-75, heat O80 ST + A (1253K/1h/WQ + 993K/16h)	None	Air	0.83 x10^{-3}	716	1130	22	---	51	[17]
	(3)	172 MPa H_2		723	1137	16	---	24	
JBK-75, heat O80 8% CW + A (948K/8h)	None	Air	0.83 x10^{-3}	1083	1302	11	---	45	[17]
	(3)	172 MPa H_2		1089	1295	12	---	18	
JBK-75 ST + A (1253K/1h/WQ + 1013K/8h)	None	Air	0.017 mm/s†	763	1109	---	29	58	[20]
	(4)	Air		763	1110	---	26	43	
JBK-75 A (1013K/8h)	None	Air	0.017 mm/s†	759	1090	---	32	59	[32]
	(5)	Air		745	1071	---	31	40	

† when strain rate is not known, displacement rates are quoted if reported
ST = solution treatment, A = age, WQ = water quench, CW = cold work (diameter reduction)

(1) 24 MPa hydrogen gas, 475 K, 100 h (gauge diameter = 3 mm); calculated concentration gradient of 45 to 4 wppm hydrogen surface to center (2500 to 250 appm)
(2) 69 MPa hydrogen gas, 473 K, 158 h (gauge diameter = 5 mm); calculated concentration gradient of 45 to 9 wppm hydrogen surface to center (2500 to 500 appm); however vacuum extraction indicated hydrogen concentration of about 20% higher
(3) 69 MPa hydrogen gas, 473 K, 240 h (gauge diameter = 5 mm); calculated concentration gradient of 99 to 2 wppm hydrogen surface to center (5500 to 100 appm)
(4) 10 MPa hydrogen gas, 573 K, 340 h (gauge diameter = 5 mm); 25 wppm hydrogen (1400 appm) measured by ion-microprobe sectional hydrogen analysis
(5) 10 MPa hydrogen gas, 573 K, 340 h (gauge thickness = 2 mm); 25 wppm hydrogen (1400 appm) measured by ion-microprobe sectional hydrogen analysis

Table 3.1.1.3. Smooth tensile properties of JBK-75 stainless steel as a function of temperature; with internal hydrogen (measured in air after thermal precharging in hydrogen gas).

Material	Thermal precharging	Test environment	Strain rate† (s^{-1})	S_y (MPa)	S_u (MPa)	El_u (%)	El_t (%)	RA (%)	Ref.
JBK-75 ST + A (1253K/1h/WQ + 1013K/8h)	None	Air 293 K	0.17 mm/s†	763	1109	---	28.9	58.1	[20]
	(1)			763	1110	---	26.1	43.4	
	None	Air 223 K		778	1152	---	30.2	57.7	
	(1)			775	1153	---	29.6	51.4	
	None	Air 153 K		806	1190	---	31.3	57.3	
	(1)			793	1207	---	33.1	56.3	
	None	Air 77 K		876	1412	---	41.6	60	
	(1)			868	1417	---	41.6	59.2	

† when strain rate is not known, displacement rates are quoted if reported
(1) 10 MPa hydrogen gas, 573 K, 340 h (gauge diameter = 5 mm); 25 wppm uniform hydrogen (1400 appm)

Table 3.1.1.4. Smooth tensile properties of JBK-75 stainless steel at room temperature as function of surface deformation due to machining; with internal hydrogen (measured in air after thermal precharging in hydrogen gas).

Material	Thermal precharging	Test environment	Strain rate (s^{-1})	S_y (MPa)	S_u (MPa)	El_u (%)	El_t (%)	RA (%)	Ref.
JKB-75, heat B80 Age† + machine	None	Air	0.33×10^{-3}	702	1105	18.2	23.4	45.3	[15]
	(1)	Air		703	1100	16.5	16.7	20.2	
JBK-75, heat B80 Age† + machine + grind	None	Air		702	1121	18.6	23.6	49.0	
	(1)	Air		716	1106	15.8	16.2	23.8	
JBK-75, heat B80 Machine + age† + grind	None	Air		806	1124	18.6	23.7	46.5	
	(1)	Air		805	1090	11.7	12.0	14.7	

† 993K/16h
(1) 69 MPa hydrogen gas, 473 K, 158 h (gauge diameter = 5 mm); calculated concentration gradient of 45 to 9 wppm hydrogen surface to center (2500 to 500 appm); however vacuum extraction indicated hydrogen concentration about 20% higher.

Table 3.1.2.1. Notched tensile properties of A-286 stainless steel at room temperature; measured in external hydrogen gas.

Material	Specimen	Thermal precharging	Test environment	Displ. rate (mm/s)	S_y † (MPa)	σ_s (MPa)	RA (%)	Ref.
A-286, heat W69 ST + A (1173K/2h/WQ+ 993K/16h/AC)	(a)	None	69 MPa He	0.7 x10^{-3}	848	1606	5.6	[10, 31]
		None	69 MPa H_2		---	1565	6.2	
A-286, heat V96 ST + A (1266K/1h/WQ+ 994K/16h/AC)	(b)	None	34 MPa He	0.21 x10^{-3}	843	1826	---	[14]
		None	34 MPa H_2		839	1756	---	

ST = solution treatment, A = age, WQ = water quench, AC = air cool

† yield strength of smooth tensile specimen

(a) V-notched specimen: 60˚ included angle; minimum diameter = 3.81 mm; maximum diameter = 7.77 mm; notch root radius = 0.024 mm. Stress concentration factor (K_t) = 8.4.

(b) Notch (minimum) diameter = 6.35 mm. Stress concentration factor (K_t) = 6.0.

Table 3.2.1.1. Fracture toughness of JBK-75 stainless steel at room temperature; measured in air with internal hydrogen (thermal precharging in hydrogen gas).

Material	Test method	Thermal precharging	Test environment	S_y (MPa)	K_Q† (MPa m$^{1/2}$)	Ref.
JBK-75, heat B80 ST + A (1253K/1h/WQ + 993K/16h)	WOL J-integral	None	Air	717	139	[36, 40]
	3PB J-integral	(1)	Air	723	77	
JBK-75, heat O80 HERF + A (1253K; 948K/8h + 873K/8h)	3PB J-integral	None	Air	937	99	[26]
		(1)	Air	---	44	
JBK-75, heat O80 HERF + A (1253K; 948K/32h)	3PB J-integral	None	Air	960	89	[26]
		(1)	Air	---	41	
JBK-75, heat O80 HERF + A (1253K; 948K/96h)	3PB LEFM	None	Air	964	87	[26]
		(1)	Air	---	35	

HERF = high energy rate forging, A = age, ST = solution treatment, WQ = water quench, WOL = wedge open loading specimen, 3PB = 3-point bending specimen, LEFM = linear elastic fracture mechanics

† not clear if plane strain requirements are met in these studies

(1) 138 MPa hydrogen, 573 K, 1500 h; estimated uniform hydrogen concentration of 120-140 wppm (6700 - 8000 appm) [36, 40]

Table 3.2.2.1. Threshold stress intensity factor for A-286 and JBK-75; measured in external hydrogen gas. The testing procedure is believed to have satisfied the requirements of ASTM E 1681-99 [28].

Material	S_y † (MPa)	RA † (%)	Threshold Stress Intensity Factor (MPa m$^{1/2}$)		Ref.
			100 MPa H_2	200 MPa H_2	
A-286, heat P81 ST +A (1253K/1h/WQ + 993K/16h)	779	46	---	94*	[19] ‡
JBK-75, heat P80 ST + A (1253K/1h/WQ + 993K/16h)	717	51	44	47	[19] ‡
JBK-75, heat P80 HERF + A (1243K/WQ + 948K/8h + 873K/8h)	855	37	109*	116*	[19] ‡
JBK-75, heat P80 HERF + A (1243K/WQ + 948K/32h)	923	38	69	66	[19] ‡
JBK-75, heat P80 Fusion weld + A (948K/8h + 873K/8h)	~700	---	~50 (H_2 pressure not reported)		[19] ‡

HERF = high-energy rate forging, ST = solution treatment, A = age, WQ = water quench
* did not satisfy plane strain requirements for analysis of linear elastic fracture mechanics
† yield strength and reduction in area of smooth tensile specimen, not exposed to hydrogen
‡ data also reported in Ref. [13, 18, 41]

Table 4.2.1. Smooth tensile properties of JBK-75 stainless steel at room temperature as a function of aging time and cold-work; measured in external hydrogen gas with internal hydrogen (thermal precharging in hydrogen gas).

Condition	Aging time	Thermal precharging	Test environment	Strain rate	S_y (MPa)	S_u (MPa)	El_u (%)	El_t (%)	RA (%)	Ref.
JBK-75, heat O80 ST + A (1253K/ 1h/WQ; 993K)	ST	None	Air	0.83 x 10^{-3} s^{-1}	241	620	35	---	70	[17]
		(1)	172 MPa H_2		245	618	34	---	67	
	4 h	None	Air		565	1058	26	---	61	
		(1)	172 MPa H_2		560	1012	18	---	24	
	8 h	None	Air		632	1091	24	---	57	
		(1)	172 MPa H_2		640	1063	16	---	23	
	12 h	None	Air		672	1131	22	---	51	
		(1)	172 MPa H_2		683	1092	16	---	21	
	16 h	None	Air		716	1130	22	---	51	
		(1)	172 MPa H_2		723	1137	16	---	24	
JBK-75, heat O80 8% CW + A (948 K)	1 h	None	Air		987	1169	13	---	60	
		(1)	172 MPa H_2		1054	1216	12	---	25	
	4 h	None	Air		1100	1288	11	---	52	
		(1)	172 MPa H_2		1136	1282	10	---	23	
	8 h	None	Air		1083	1302	11	---	45	
		(1)	172 MPa H_2		1089	1295	12	---	18	
JBK-75, heat O80 20% CW + A (948K)	1 h	None	Air		1196	1306	6.9	---	54	
		(1)	172 MPa H_2		1226	1325	7.8	---	31	
	4 h	None	Air		1178	1340	8.5	---	45	
		(1)	172 MPa H_2		1192	1326	9.2	---	22	
	8 h	None	Air		1085	1304	9.5	---	40	
		(1)	172 MPa H_2		1123	1295	9.6	---	19	
JBK-75, heat O80 36% CW + A (948K)	1 h	None	Air		1212	1337	5.8	---	50	
		(1)	172 MPa H_2		1240	1350	7.2	---	21	
	4 h	None	Air		1029	1269	10	---	44	
		(1)	172 MPa H_2		1075	1268	9.5	---	19	
	8 h	None	Air		785	1169	15	---	48	
		(1)	172 MPa H_2		878	1152	12	---	20	

ST = solution treatment, A = age, WQ = water quench; CW = cold work (diameter reduction)
(1) 69 MPa hydrogen gas, 473K, 240 h (gauge diameter = 5 mm): calculated concentration gradient of approximately 99 to 2 wppm hydrogen surface to center (5500 to 100 appm)

Table 4.3.1. Smooth tensile properties of JBK-75 composite GTA weld specimens at room temperature; with internal hydrogen (measured in air after thermal precharging in hydrogen gas), or measured in external hydrogen gas with internal hydrogen (thermal precharging in hydrogen gas).

Material	Thermal precharging	Test environment	Strain rate (s^{-1})	S_y (MPa)	S_u (MPa)	El_u (%)	El_t (%)	RA (%)	Ref.
JBK-75, heat B83w†	None	Air	0.33×10^{-3}	781	1014	6.0	8.2	38	[21]
	(1)	Air		749	980	4.6	4.8	24	
Aged (948K/8h + 873K/8h)	(2)	Air		796	993	4.2	4.4	22	
	(2)	172MPa H_2		760	953	4.6	5.0	23	

† The base material for these studies was HERF (high energy rate forging), back extrusions of JBK-75, machined to cylindrical shape (10 mm diameter, 1.5 mm wall thickness) with circumferential double J grooves; eight to ten weld passes were required to fill groove. The filler material was also JBK-75 matched to the composition of the base metal. Tensile bars contain base material and heat affected zone with the fusion zone centered in the gauge length, and were aged after machining.

(1) 24 MPa hydrogen gas, 473 K, 240 h (gauge diameter = 5 mm): calculated concentration gradient of 45 to 4 wppm surface to center (2500 to 200 appm)

(2) 69 MPa hydrogen gas, 473 K, 240 h (gauge diameter = 5 mm): calculated concentration gradient of 72 to 7 wppm surface to center (4000 to 400 appm)

Table 4.3.2. Smooth tensile properties of JBK-75 EB-weld specimens at low temperatures; with internal hydrogen (measured in air after thermal precharging in hydrogen gas).

Material	Thermal precharging	Test temperature (K)	Strain rate† (s^{-1})	S_y (MPa)	S_u (MPa)	El_u (%)	El_t (%)	RA (%)	Ref.
JBK-75 Aged (1013K/8h)	None	293	0.017 mm/s†	759	1090	---	32	59	[32]
	(1)			745	1071	---	31	40	
JBK-75 EB welds Aged (1013K/8h)	None	293		800	1041	---	18	52	
	(1)			784	1032	---	16	33	
	None	193		826	1096	---	19	51	
	(1)			832	1121	---	20	44	
	None	77		909	1306	---	25	50	
	(1)			921	1318	---	24	41	

EB = electron beam

† when strain rate is not known, displacement rates are quoted if reported

(1) 10 MPa hydrogen gas, 573 K, 340 h (gauge thickness = 2 mm); 25 wppm hydrogen (1400 appm) in the base metal and 16 wppm (920 appm) in the weld metal, measured by ion-microprobe sectional hydrogen analysis

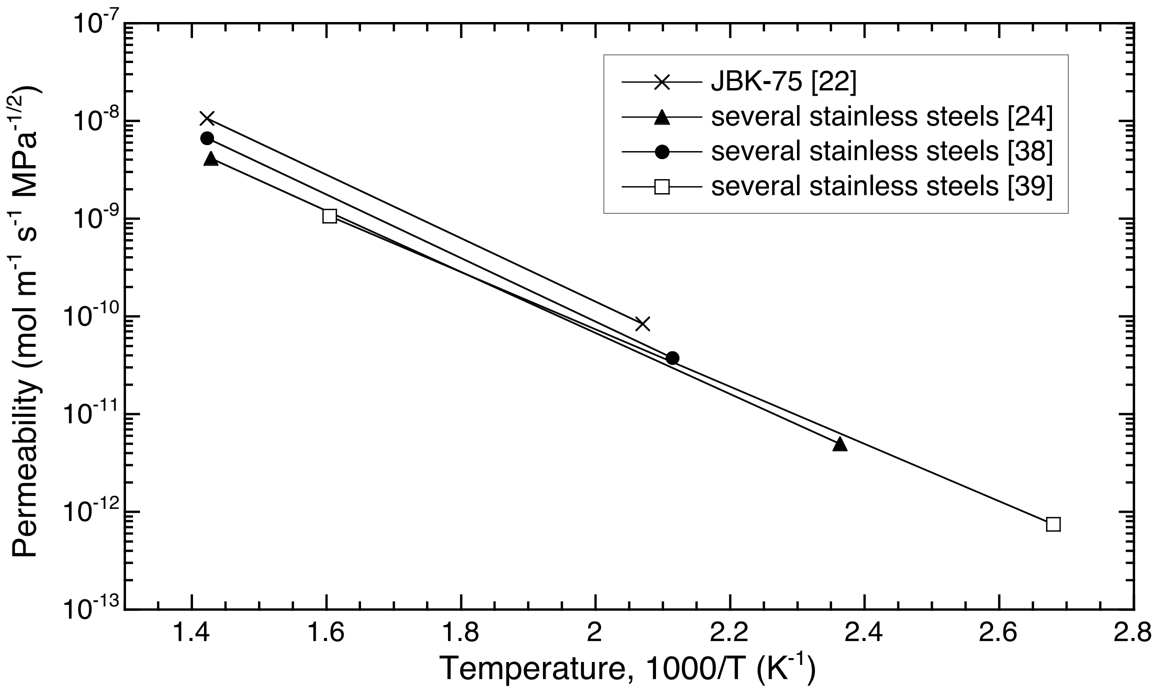

Figure 2.1. Permeability in JBK-75 and average relationships determined for several austenitic stainless steels. Data from Ref. [24] is determined for deuterium: permeability has been corrected here to give permeability of hydrogen by multiplying by the square root of the mass ratio ($\sqrt{2}$).

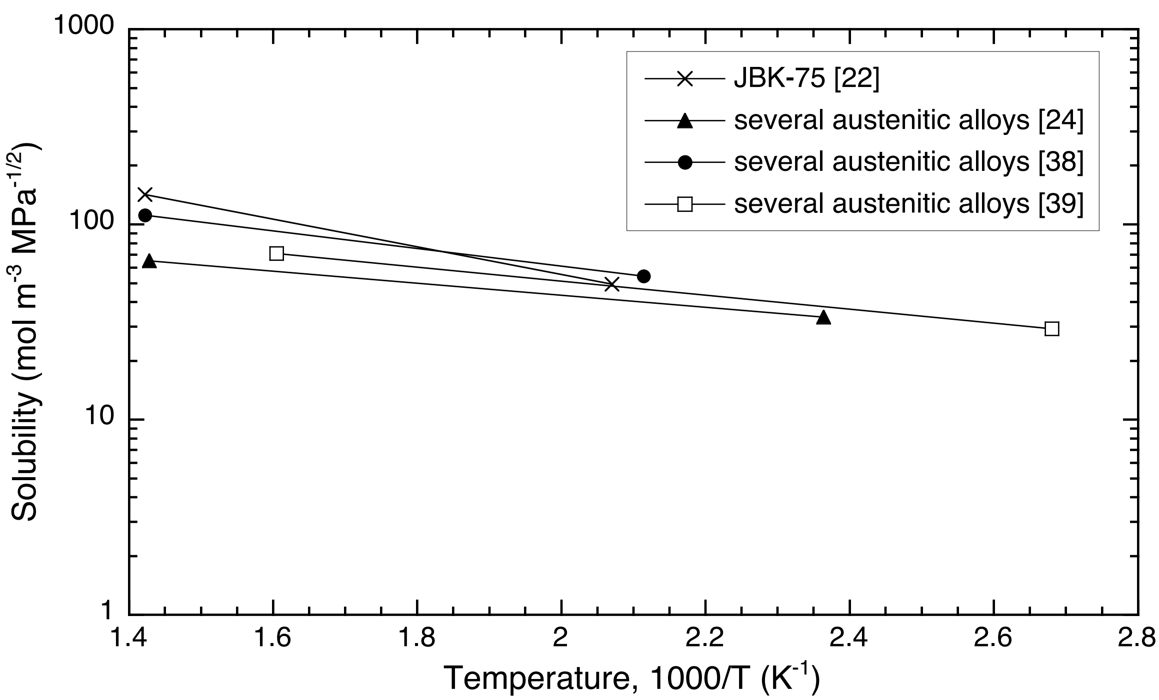

Figure 2.2. Solubility in JBK-75 and average relationships determined for several austenitic stainless steels. Data from Ref. [24] is determined for deuterium; however, solubility is assumed to be independent of hydrogen isotope.

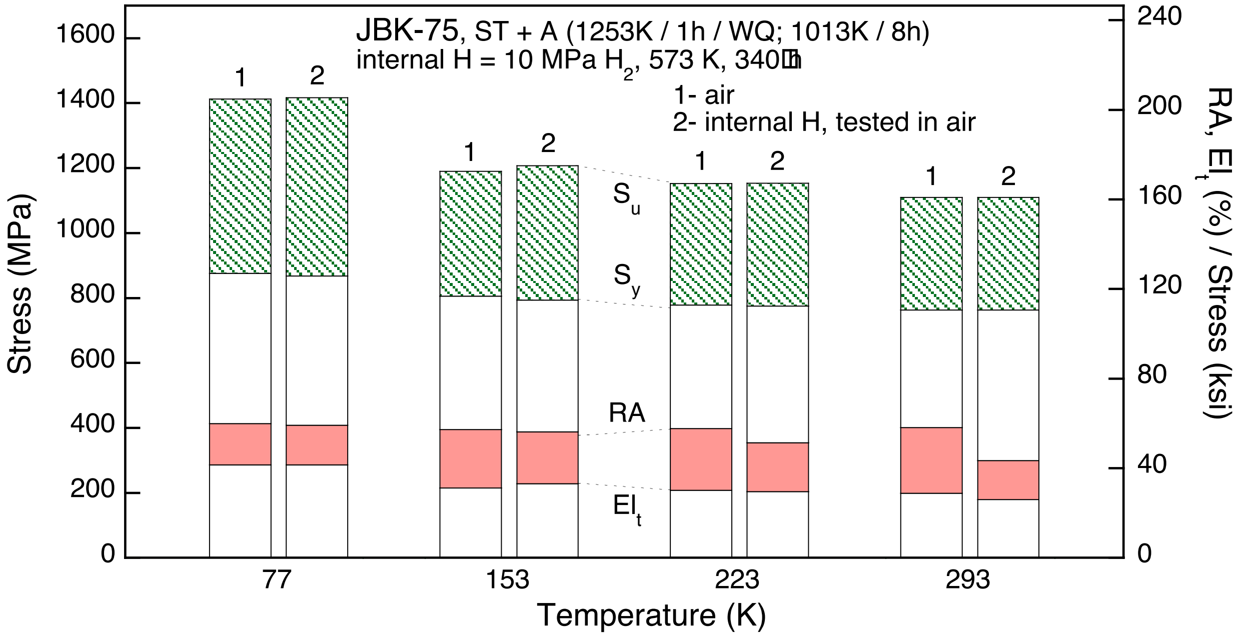

Figure 3.1.1.1. Smooth tensile properties of JBK-75 stainless steel as a function of temperature; with internal hydrogen (measured in air after thermal precharging in hydrogen gas). Data also presented in Table 3.1.1.3. [20]

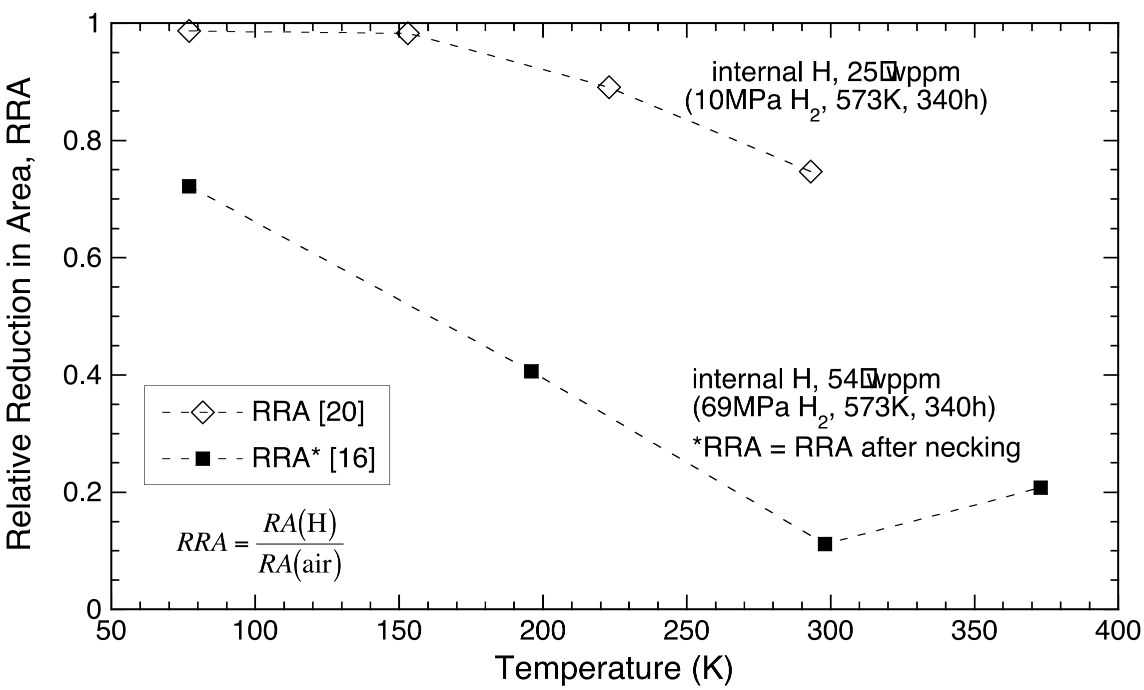

Figure 3.1.1.2. Relative reduction of area (RRA) of smooth tensile specimens of JBK-75 stainless steel as a function of temperature; with internal hydrogen (measured in air after thermal precharging in hydrogen gas). Data from Ref. [20] is also presented in Table 3.1.1.3 and Figure 3.1.1.1.

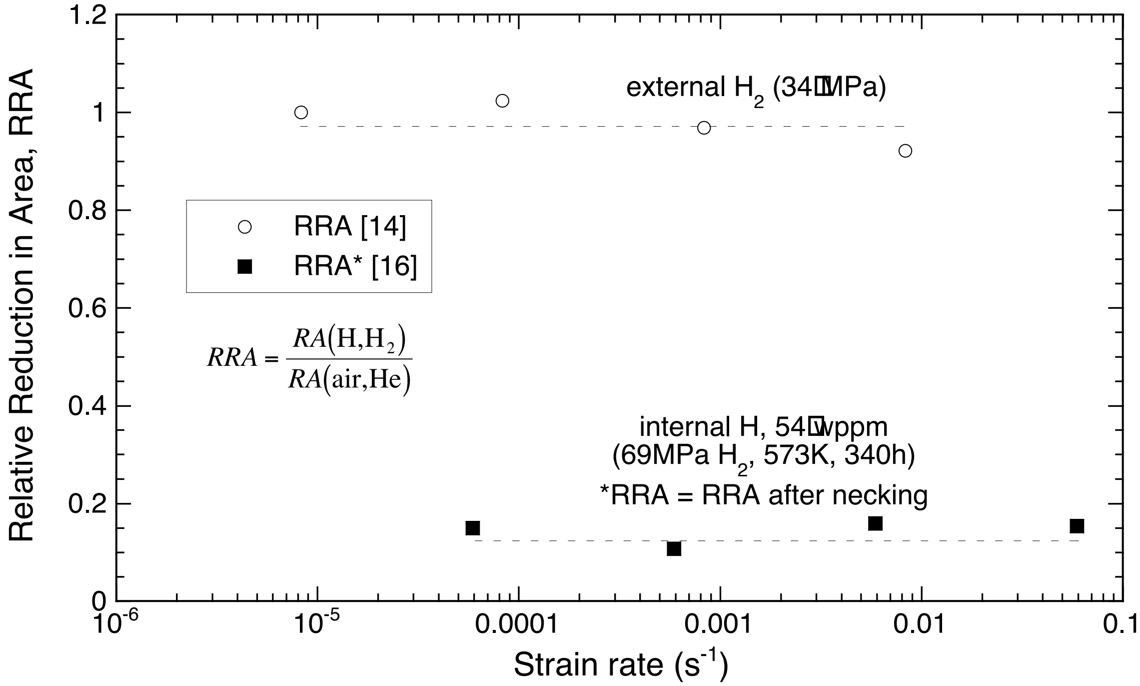

Figure 3.1.1.3. Relative reduction in area of smooth tensile specimens of JBK-75 stainless steel at room temperature as a function of strain rate.

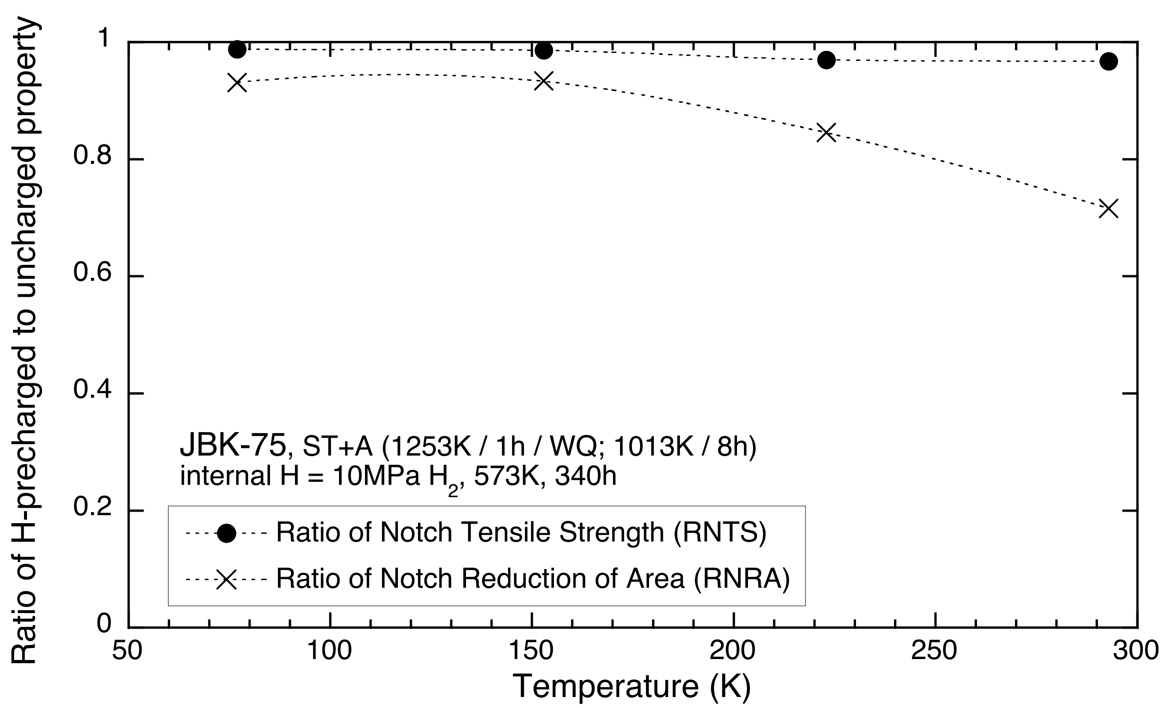

Figure 3.1.2.1. Notched tensile properties of JBK-75 stainless steel as a function of test temperature; measured in air with internal hydrogen (thermal precharging in hydrogen gas). [20]

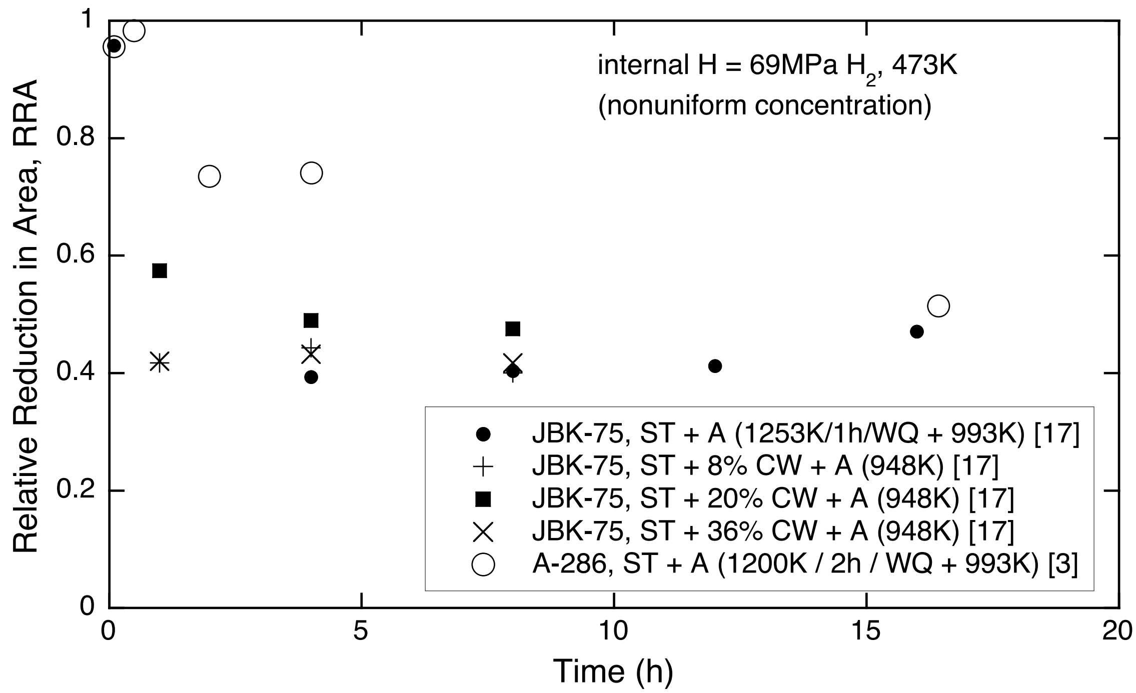

Figure 4.2.1. Relative reduction of area (RRA) as a function of aging time for several microstructural conditions of JBK-75; measured in external (172 MPa) H_2 gas with internal hydrogen (heat O80), data also reported in Table 4.2.1, and for A-286 with internal hydrogen (heat B93). ST = solution treatment, A = age, WQ = water quench, CW = cold work

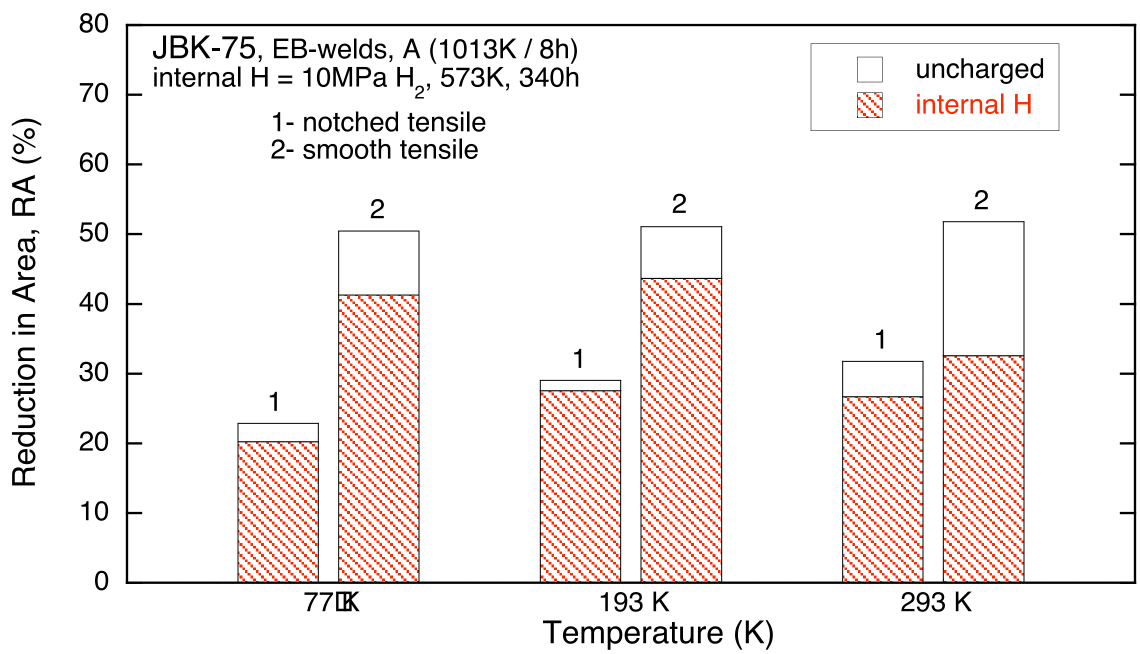

Figure 4.3.1. Reduction in area of JBK-75 stainless steel EB-welded joints as a function of test temperature; measured in air with internal hydrogen (thermal precharging in hydrogen gas). [32] EB = electron beam, A = age